

Synthesis of nanocrystalline silicon using the recrystallisation of binary silica cryogel/Mg system via self-propagating high-temperature combustion in the presence of NaCl as a metal halide diluent

Mahya Nangir, Abouzar Massoudi , Rahim Yazdanirad, Seyed Ali Tayebifard

Semiconductors Department, Materials and Energy Research Center, P.O. Box 14155/4777, Tehran, Iran

✉ E-mail: massoudi@merc.ac.ir

Published in Micro & Nano Letters; Received on 25th April 2017; Revised on 8th September 2017; Accepted on 29th September 2017

Self-propagating high-temperature synthesis as a low energy consumption and simple approach was employed to synthesise silicon nanocrystal from the monolithic silica cryogel prepared by freeze drying. The recrystallisation process of silicon was investigated under combustion at 800, 900 and 1000°C and the uniform coral-like structure was achieved at 1000°C. The results of Raman and X-ray diffraction analysis showed the decrease in ignition time to 40 s for 1000°C temperature, leading to the decrement of crystalline size to 10.85 Å and the raise of average lattice strain to 0.152% due to accelerating recrystallisation. In addition, NaCl diluent consumed the excess heat generated during exothermic reaction and decreased the crystalline size to 10.79 Å thanks to its 0.8 W/m K thermal conductivity.

1. Introduction: Silicon, the second most abundant element in the Earth's crust, has attracted great attention in electronic applications such as energy conversion and storage devices, owing to its unique set of physical and chemical properties. Thanks to its wide indirect bandgap (>1.12 eV), silicon nanocrystal is a suitable absorbing material for solar cells [1]. In addition, it is considered as a promising anode material for next generation lithium ion batteries [2].

Self-propagating high-temperature synthesis (SHS), also known as combustion synthesis, is an energy-efficient, fast, simple and low-cost method to produce oxidative, non-oxidative compounds and pure metals for various industries including but not limited to catalysis, cutting tools and corrosion [3–5]. Historically, Merzhanov discovered SHS to synthesise nanopowders in a gasless combustion system [6]. In general, SHS method, depending on physical nature of raw materials, is divided into three main types: condensed-phase combustion (CPC), which is a common method in self-combustion synthesis of solid reactants [7]; solution-combustion synthesis, which is a self-sustaining process used for various oxidisers (e.g. chlorates) and fuels (e.g. glycol) in homogeneous solutions [8]; and gas-phase combustion, which is generally used for nitridation processes at high pressures [9].

Although preparing different pure compounds with specific stoichiometry is the most important property of CPC [7], particle growth and agglomeration is a dominant phenomenon in high-temperature synthetic manners.

Different regulating additives or diluents play a crucial role to form the fine and ultrafine structures through controlling the adiabatic temperature and the rate of ignition reaction [9]. Generally, diluents based on its performance mechanism have been classified into three types of pure metals, carbonates and metal halides [10]. Pure elemental metallic diluents such as aluminium result in decelerate reaction. In this way, the consubstantial metallic diluent with a main product is used to avoid undesirable byproducts. In the reactant mixture containing a large particle of diluent, heat sinks between grain boundaries lead to the increment of reaction time due to the slow combustion rate. On the other hand, existence of unreacted additive particles diminishes the homogenous morphology [10].

Carbonates are other useful regulating additives that consume the excess heat generated in thermal reactions. Indeed, thermodynamically, decomposing covalent bonds between carbon and oxygen in solid-state redox reactions requires a high amount of free energy.

Hence, using these compounds as a diluent in reactant mixture consumes the excess heat of reaction and controls the combustion rate before self-decomposing [9]. Carbon–oxygen bonds in low temperature processes, owing to the low exothermicity of reaction, cannot be decomposed and remains as an impurity in the product. While, in high temperature synthetic methods, increasing reaction rate can be associated with decomposition of carbon content to form the released CO and CO₂, resulting in the creation of porosity in the structure and decrease product density [10].

Metal halides (or alkaline salts) with low melting points, within 600–800°C, have been known as the most interested diluent for controlling the combustion reaction rate. When the mixture is combusted at a temperature higher than 2000 K, alkaline salts are melted and diffused between interface particles of reactant, consuming the generated heat and preventing the rising combustion temperature and crystal growth. The product grain size can be controlled by varying the diluent content [11].

Thermodynamically, the SHS process is an exothermic and a self-sustaining chemical reaction. When an explosion occurs, combustion temperature increases to adiabatic temperature under adiabatic conditions, resulting in enthalpy difference between reactants and products. Meanwhile, the reaction heats, $\Delta H_{T_{ad}}^{\circ}$, are calculated by the following relationship [12]:

$$\Delta H_{T_{ad}}^{\circ} = \Delta H_{298}^{\circ} + \int_{298}^{T_{ad}} \sum n_f C_p(\text{product}) dT \quad (1)$$

where the $\Delta H_{T_{ad}}^{\circ}$, ΔH_{298}° , n_f and C_p are the *standard enthalpy of reaction at adiabatic temperature*, the enthalpy of the reaction at room temperature (298 K or 25°C), the reaction stoichiometry coefficient and the heat capacity of product, respectively. It should be noticed that $\Delta H_{T_{ad}}^{\circ}$ is always zero under adiabatic conditions. There are two important conditions for a self-propagating mode in the combustion reaction. First, the standard enthalpy threshold of a reaction must be $\Delta H_{298}^{\circ} = -168$ kJ/mol, and second, the ratio of $\Delta H_{298}^{\circ} / \sum n_f C_p$ 2000 K or $T_{ad} > 1800$ K [12]. Absence of the least one of above conditions will prevent the combustion reaction. In this case, the reactions require pre-activation, e.g. chemical oven [13], ball milling process [14] and so on. Mechanical activation based on collision between particles either together or with the cup wall creates numerous defects in their surface, which results in an enhance in the activation energy.

Therefore, products are synthesised at a lower ignition temperature and a higher combustion velocity [15].

Herein, regulated silicon nanocrystals have been synthesised in the presence of NaCl via SHS method. The effect of ignition temperature on recrystallisation process has been investigated as well as crystallinity and morphology of the samples. Furthermore, the mechanism of homogenous structure formation and the crystallite growth has been explained.

2. Experimental

2.1. Materials: Tetraethyl orthosilicate (TEOS, 99.98%, Merck, German) and ammonium hydroxide (NH₄OH, 28%, Merck, German) as a surfactant were used to prepare the silica nanoparticles. Magnesium powder (0.3 mm, ≥98.5%, Merck, German) was used as a reducing agent. Commercial silicon powder (0.15 mm, >99%, Merck, German) and NaCl (≥99.9%, Merck, German) were used as an additive.

2.2. Synthesis of SiO₂ cryogel: TEOS, EtOH and deionised water were mixed at room temperature and magnetically stirred. Then, hydrogen fluoride (HF) solution was added to the mixture and sol was kept in a static condition to form a monolithic transparent gel. The molar ratio of TEOS:EtOH:H₂O:HF was 1:8:4:0.6. Afterward, the gel was aged in ethanol at room temperature for 4 days, solvent was changed with deionised water for three times, gel was immersed into the liquid nitrogen for 50 min and finally sample was kept in a freeze-drier chamber for 24 h at -55°C and 0.021 mbar.

2.3. Synthesis of silicon via MASHS method: First, commercial magnesium (Mg) powder with an average particle size of 300 μm was mechanically activated. The activation was carried out by Retsch PM100 planetary ball mill with 250 ml stainless steel cup under argon atmosphere for 1 h. The ball to powder ratio was 10:1, and 300 rpm rotation speed was used. Afterward, SiO₂:Mg with molar ratio of 1:2.5 together 10 wt% diluent were mixed and compacted under the pressure of 400 Mpa by a SVO151G5-1 uniaxial cold press. Finally, green compacts were combusted at 800, 900 and 1000°C under argon atmosphere into the tubular furnace. After synthesis, the samples were leached in 1 M HCl and 1 M HF solution for the removal of MgO and unreacted silica, respectively, then washed with deionised water and dried at 80°C for 5 h.

2.4. Structure characterisation: The powders X-ray diffraction (XRD) patterns were determined by a Phillips pw 3710 X-ray diffractometer with Co K_α radiation (λ = 1.789010 Å) at 0.02°/min at the 2θ range of 5–85°. The crystalline size of products was calculated by Scherrer formula after refining pattern via Rietveld method. A field-emission scanning electron microscope (FE-SEM) equipped with energy-dispersive X-ray spectroscopy (EDS) and MAP analysis was used to characterise morphology and chemical composition of the samples (MIRA3 TESCAN model). The diameter distribution of branches was calculated from FE-SEM images by 'Digimizer' software.

3. Results and discussion: Mechanism of silica reduction and silicon formation, schematically depicted in Fig. 1, is as follows: when the green compact of SiO₂/Mg mixture underwent a higher temperature than Mg melting point, molten magnesium diffused into pores of SiO₂ cryogel, and interface between SiO₂ and Mg particles was increased for solid-state redox reactions. Meanwhile, the additive salt was melted and nucleation of silicon was initiated in the presence of the molten salt because of the heat generated during exothermic reaction. Existence of a molten salt in the reaction prevented the agglomeration and rapid growth of particles [9]. Subsequently, Si/MgO nanocomposite was synthesised with desirable structure. During self-propagation

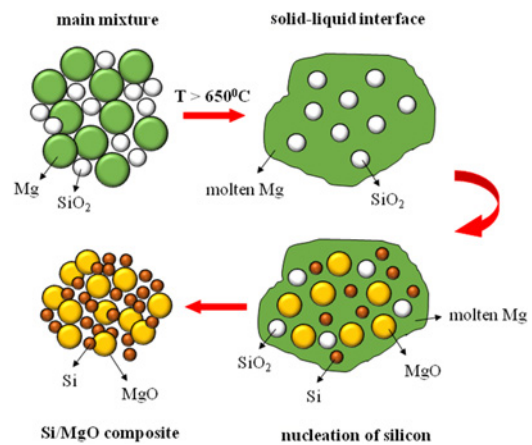
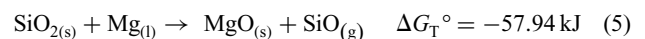
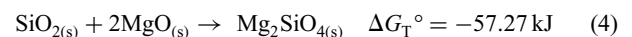
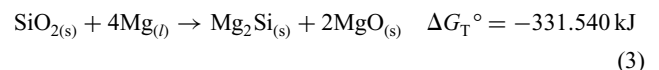
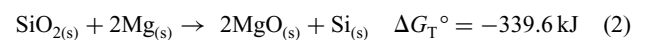


Fig. 1 Schematic diagram of the silicon fabrication during SHS process

high-temperature synthesis, reduction of the amorphous silica to crystalline silicon is followed by (2), which resulted in Si/MgO nanocomposite production [16]



The value of calculated ΔH_{298}° for combustion reaction between SiO₂ and Mg is -334.2 kJ/mol based on (1), which is much less than its threshold. Moreover, the calculated adiabatic temperature for α=2 in SiO₂+αMg binary mixture is 5942 K, which is much more than the minimum allowed adiabatic temperature that is required for a self-propagating reaction. Therefore, the reaction was exothermic and self-sustaining [14].

Fig. 2 presents the XRD patterns of silicon synthesised without additive at 1000°C before and after acid leaching. A broad peak at about 26° and the other sharp peaks at higher angles correspond to amorphous silica and crystalline Mg powder, respectively. When SiO₂/Mg mixture ignited at 1000°C, oxygen atoms removed the amorphous SiO₂ network and reacted with the molten Mg particles.

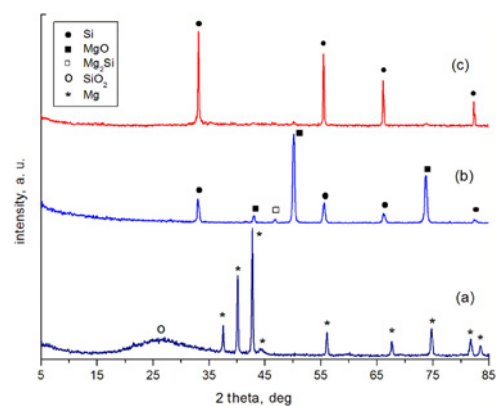


Fig. 2 XRD patterns of
a Main mixture of SiO₂ cryogel and Mg powder
b Si/MgO/Mg₂Si composite in synthesised sample at 1000°C before acid leaching
c After acid leaching

Finally, MgO was produced as a byproduct. Moreover, the atoms of liquid Mg interstitially located into the SiO₂ network leading to synthesis of Mg₂Si. Hence, a broad peak of SiO₂ and several crystalline Mg peak were removed and MgO and Mg₂Si as a byproduct and silicon as a main product (JCPDS Card No. 005-0565) was appeared. The b pattern depicts the indexed peaks of MgO, Mg₂Si and Si that MgO and Mg₂Si were completely removed by HCl leaching and remaining SiO₂ was removed by HF leaching (pattern c). Hence, the four peaks at $2\theta=33.10^\circ$, 55.48° , 66.13° and 82.44° , respectively, corresponded to (111), (220), (311) and (400) planes as well indexed to cubic silicon. In Fig. 3a, Mg₂SiO₄ was observed as a byproduct of combustion reaction between MgO and SiO₂ at 800°C (according to (4)), which shows the reduction reaction was not completely accomplished at 800°C. Mg₂SiO₄ compound is an unsolvable material in HCl and HF solutions [13]. Thus, it could not be removed by acid leaching.

3.1. Effect of ignition temperature on the crystallite growth: Fig. 3a shows the XRD patterns of silicon produced at 800–1000°C after acid leaching. The width of peaks in silicon synthesised at 800°C is lower than the width of silicon peaks at 900 and 1000°C, indicating a superior crystallinity. Fig. 3b shows the trend of the crystal growth at the four orientations, which are varied by temperature from 800 to 1000°C.

At 800°C, the crystallite size was regularly increased to 76.4, 82.7, 87.4 and 97.3 nm at (111), (220), (311) and (400) orientations, respectively, when the 2θ of XRD diffractometer was increased from 33° to 82.4° . While, at 900°C owing to

non-equilibrium nature of the reaction, the crystallites were irregularly decreased to 61.3, 53.2, 62.2 and 50.2 nm at (111), (220), (311) and (400) orientations, respectively. Once the temperature was raised to 1000°C, the crystallites size was, respectively, varied to 61.7, 66.8, 77.6 and 78.6 nm at the mentioned orientations, showing the silicon nanocrystalline. Variation of average crystallite size and lattice strain as a function of combustion temperature has been listed in Table 1. By increasing the ignition temperature from 800 to 1000°C, the average crystallite size was decreased from 85.2 to 69.4 nm that is due to the reducing reaction time from 120 to 40 s. In addition, lattice strain was increased from 0.123 to 0.152% by increasing ignition temperature, showing the increment of dislocations in crystalline structure as a result of decreasing ignition time. Hence, the largest lattice strain and the smallest crystallite size were observed at 1000°C. With raising combustion temperature to higher than 1000°C, it is predicted that the crystallinity of silicon will be decreased while the nucleation velocity will be raised. Raman spectroscopy was carried out to confirm the crystallinity of all the samples. As Fig. 3c shows, a broad peak at below 520 cm^{-1} assigned to TO mode in phonon confinement. The curves after fitting through Gaussian function showed a red shift of about $10.8\text{--}19.55\text{ cm}^{-1}$, which can be attributed to strain in the structure due to significant decline in crystalline size. The result of Zi's confinement model to calculate crystallinity of the samples revealed the role of NaCl diluent on the size reduction from 10.85 to 10.79 Å at 1000°C, as shown in Fig. 3d. Also, density of defects in silicon which was synthesised in the presence of NaCl increased to 24.42 cm^{-1} . Mechanism of crystallite size variation and lattice strain is as follows: when magnesium reacted

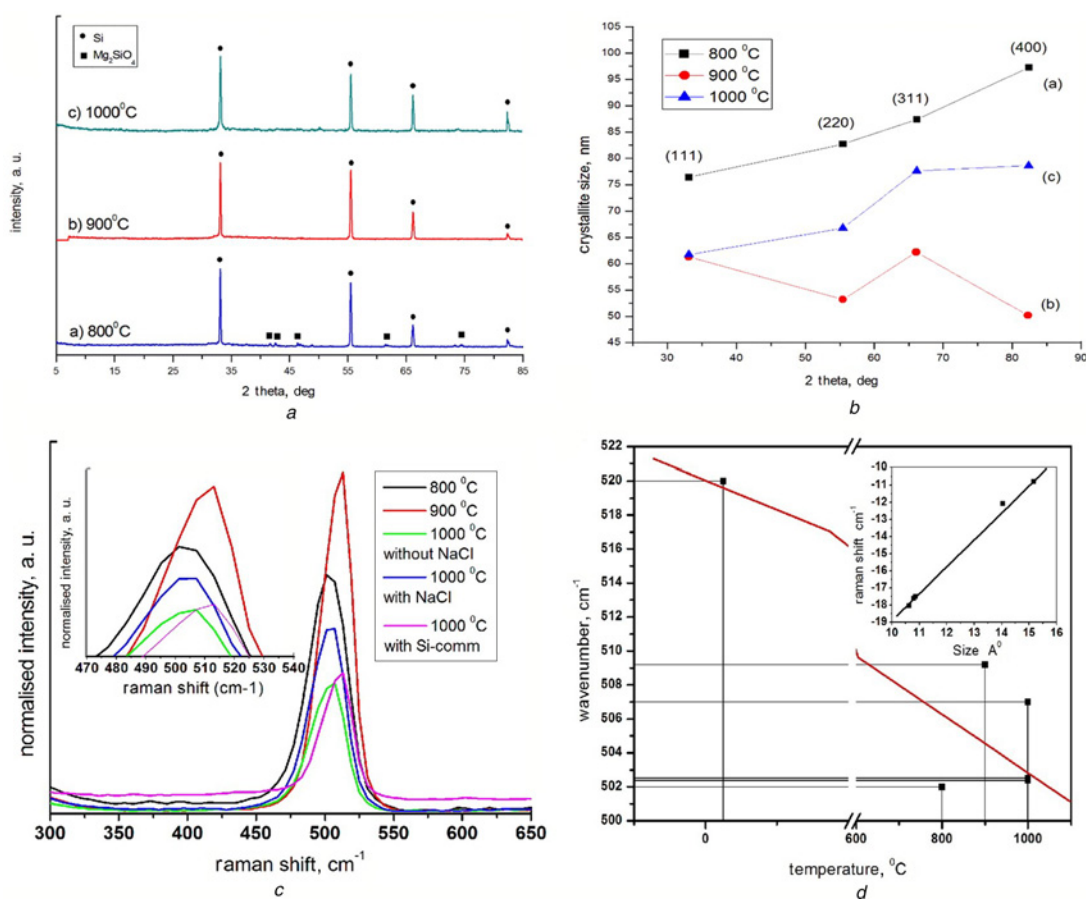


Fig. 3 Investigation of silicon crystallinity under different temperatures

a XRD patterns of the silicon after combustion at three different temperature

b Variation of crystallite size due to the changing ignition temperature in synthesised silicon at (a) 800°C, (b) 900°C and (c) 1000°C

c Red shift of silicon nanocrystals

d Variation of crystallinity as a function of temperature. The legended plot to Fig. 3d shows the decrease in crystallite size with increase in Raman shift

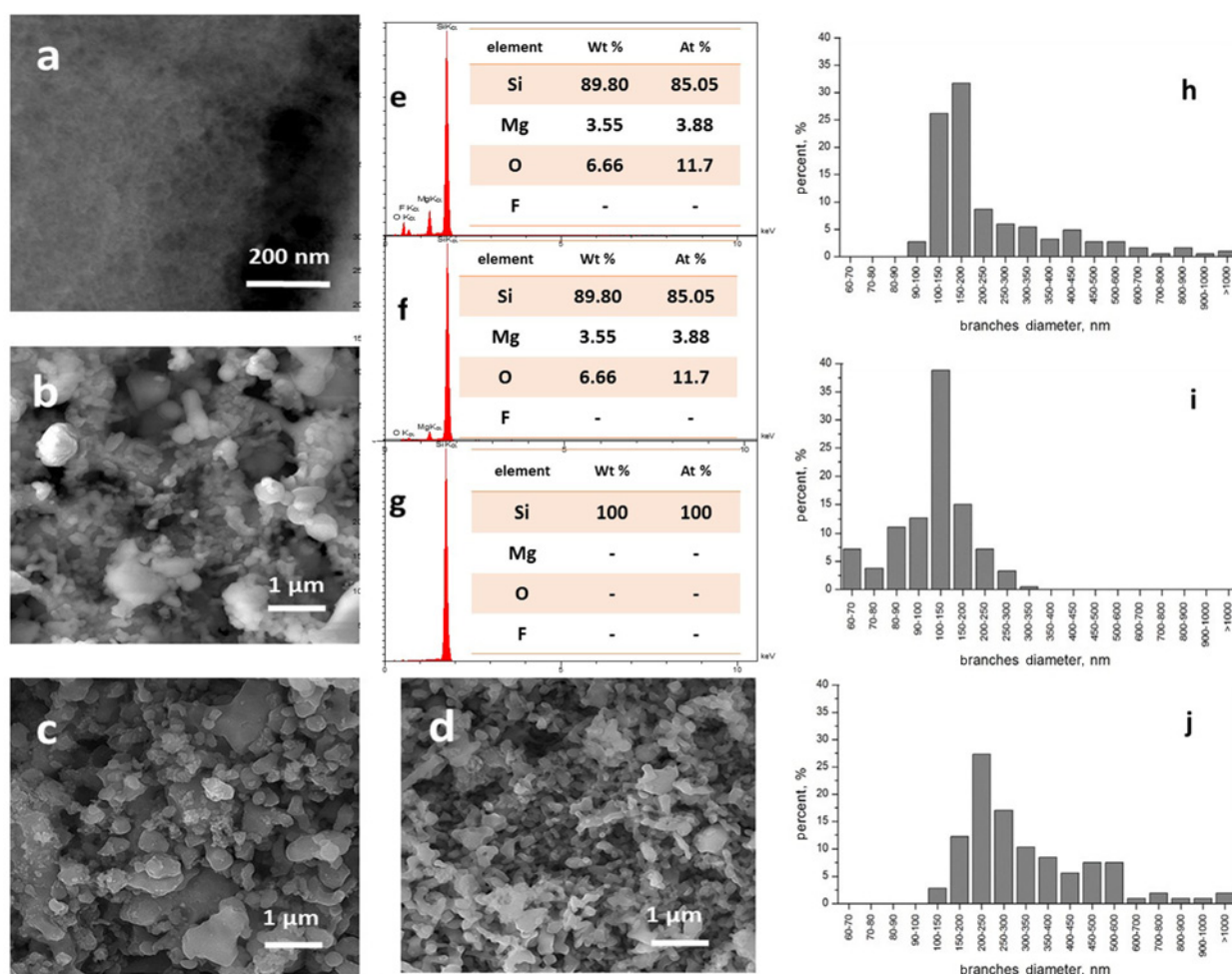
Table 1 Average crystallite size, lattice strain and average branches diameter of synthesised silicon at different conditions

Sample no.	Ignition temp., °C	Reaction time, s	Diluent (10 wt% of SiO ₂ precursor)	From XRD analysis		From Raman analysis			From FE-SEM	
				Average crystallite size, nm	Average lattice strain, %	Red shift, cm ⁻¹	FWHM	Crystallite size, Å°	Average branches diameter, nm	SD (± nm)
1	800	120	—	85.2	0.123	18.02	27.13	10.62	170	16
2	900	60	—	56.7	0.182	10.8	21.24	15.16	228	14
3	1000	40	—	69.4	0.152	17.49	24.16	10.85	122	12
4	1000	20	commercial Si	55.6	0.191	12.07	39.71	14.04	95	27
5	1000	47	NaCl	53	0.195	17.49	24.42	10.79	274	160

with silica, the amorphous silica network was rearranged and a cubic lattice of silicon crystalline was formed under recrystallisation temperature [17]. During recrystallisation of silicon, nucleation of new crystallites began. At low temperatures, increasing reaction time led to decrease of nucleation rate and growth of crystallites [17]. When the ignition temperature was increased, the growth of crystallite was controlled and numerous crystallite with smaller size were formed, which led to increase of grain boundary and

dislocation. Since each dislocation represents the crystal defect and each defect is a source of lattice strain, lattice strain was increased by decreasing crystallite size [17].

3.2. Effect of ignition temperature on the product morphology: Fig. 4a illustrates the micrograph of as-synthesised silica cryogel with spongy-like structure. The freezing under −55°C temperature and 0.021 mbar pressure to dry the gel resulted in

**Fig. 4** Evolution of product microstructure under three different combustion temperature

a FE-SEM micrographs of SiO₂ cryogel precursor
b Silicon synthesised at 800°C after MASHS process
c Silicon synthesised at 900°C after MASHS process
d Silicon synthesised at 1000°C after MASHS process
e EDS spectra of prepared products at 800°C
f EDS spectra of prepared products at 900°C
g EDS spectra of prepared products at 1000°C
h, i, j Size distribution of branches diameter in coral-like structure formed at 800, 900 and 1000°C, respectively

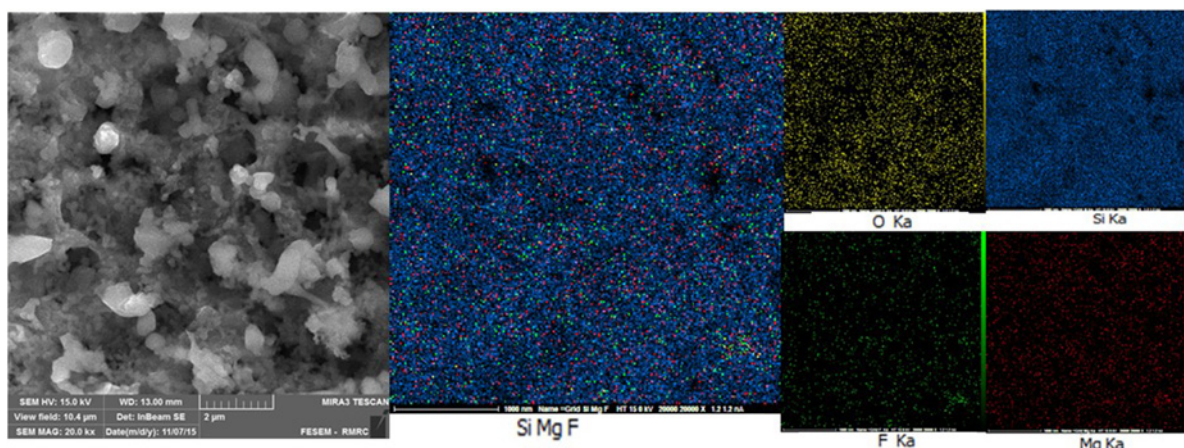


Fig. 5 Micrograph of morphology and elemental distribution of prepared product at 800°C via MASHS method
a FE-SEM image
b, c EDS mapping of this sample

decrease of the surface tension and the formation of monolithic spongy-like silica cryogel, that is in agreement with Pons [18]. The microstructure images of silicon synthesised at 800, 900 and 1000°C in Figs. 4*b–d* reveals the independence on precursor morphology. As seen in Fig. 4, all three products have the coral-like morphology with many irregular branches. The surface of branches is very smooth and their distribution is approximately homogenous except the grown up branches at 800°C. At 800°C, as seen in Fig. 4*b*, the several branches were agglomerated due to the high reaction time (120 s in comparison to 60 s for 900°C and 40 s for 1000°C). Fig. 4*h* illustrates that 32% of grown up branches at 800°C have the diameter size distribution in the range of 150–200 nm. While, the finer branches and the agglomerated branches were also formed with diameter size distributions in the ranges of 100–150 and 200–450 nm. Nonetheless, the average diameter of major branches was measured to be 170 nm. Moreover, Fig. 5 depicts the result of MAP analysis on the sample ignited at 800°C, which represents the several covered silicon branches by Mg_2SiO_4 . However, amount of coverage and existence of Mg_2SiO_4 is negligible, which is consistent with the XRD and EDS results. Increasing ignition temperature to 900°C led to growth of branches due to reaction exothermicity. Thereby, the coarse branches grew up uniformly throughout the sample. The diameter size distribution of coarse branches is shown in Fig. 4*i*. The results reveal that the average diameter of branches possess an approximately normalised distribution, ranging from

150 to 600 nm. In addition, it can be found in Fig. 4*i* that 27% of the branches with the highest nucleation in the formed coral-like structure have a diameter size distribution in the range of 200–250 nm with average size around 228 nm. Once the temperature was raised to 1000°C, the number of germinated branches was increased with the least possible growth due to reduction of reaction time to 40 s, which led to observation of uniform and homogenous coral-like structure. Thus, the diameter size in 40% of sub-micron branches was in the range of 100–150 nm with the average size of 122 nm (see Fig. 4*j*). It can be predicted that with raising the reaction temperature to above 1000°C, the average size of the major branches will be declined to lower than 122 nm and also homogeneity of its structure will be improved. According to the EDS spectrum of every silicon synthesised at three different temperatures shown in Figs. 4*e–g*, all of the samples included Si element in their EDS spectrum. At 800°C, a small percentage of Mg, O and F elements were observed in the sample. While, the enhancement of temperature led to relative decrease of Mg and O element at 900°C and removal of Mg, O and F elements at 1000°C. The weight and atomic per cent of the constituent elements of each sample are listed in legended table of every EDS spectrum.

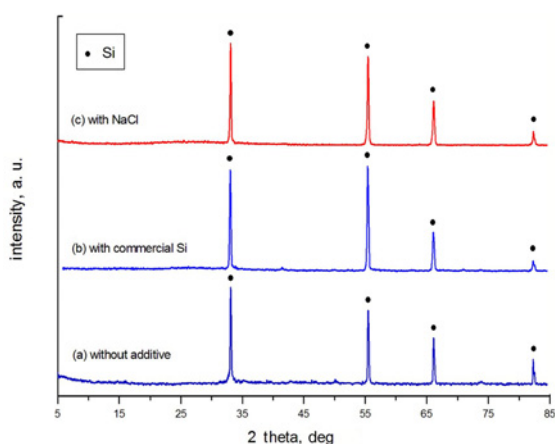


Fig. 6 XRD patterns correspond to investigate the purity products
a In the absence of a diluent
b In the presence of commercial silicon diluent
c In the presence of NaCl diluent

3.3. Effect of the diluent: As the mentioned in Section 3.2, the average crystallite size of silicon was raised to 56.7 at 900°C and 69.4 nm at 1000°C. Moreover, the homogeneous popular morphology was achieved at 1000°C. Therefore, the diluent was added to the main mixture at 1000°C to synthesise the homogeneous coral-like silicon with the lowest crystallite size. Fig. 6 shows the XRD patterns of silicon synthesised with two different diluents at 1000°C to compare with silicon synthesised without the diluent at the same temperature. Silicon at two different conditions was well synthesised without any impurity. As previously observed in Table 1, the high temperature (1000°C) led to the growth of crystallite with the average size of 69.4 nm. While, the average crystallite size was decreased to 53.8 and 55.6 nm when 10 wt% equal 0.05 g NaCl and commercial silicon were used, respectively, as the diluent in SiO_2/Mg mixture at the same temperature. During combustion reaction, NaCl with 0.8 W/m K thermal conductivity as a diluent was melted at a temperature higher than its melting point (801°C) and was diffused between silicon synthesised particles and post-combustion zone. Therefore, heat generated during exothermic reaction was consumed and prevented the crystallite growth. Elsewhere, the various inhibitors were used to prevent the crystallite growth and decreasing the particles size [11]. Fig. 7 depicts the micrograph of silicon synthesised in the presence of

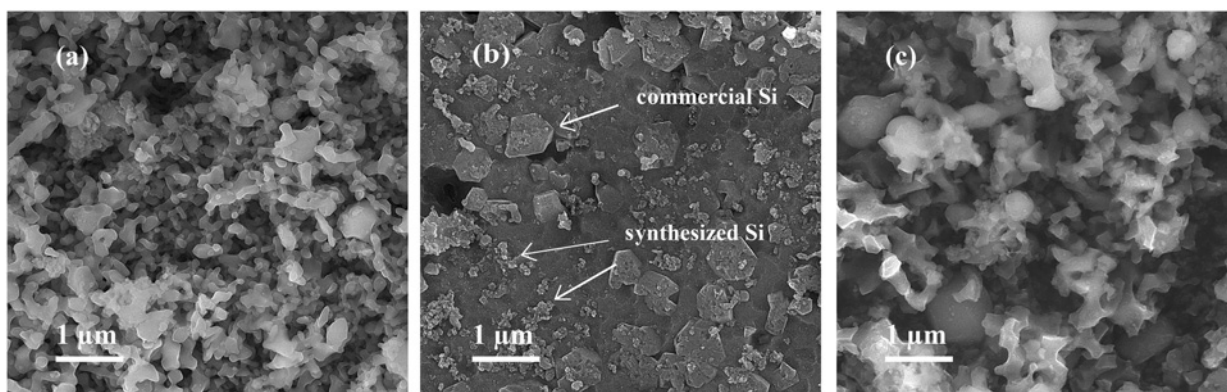


Fig. 7 FE-SEM micrographs of silicon synthesised at 1000°C

a In the absence of diluent

b In the presence of commercial silicon diluent

c In the presence of NaCl diluent after MASHS process

NaCl and commercial silicon diluents at 1000°C to compare with synthesised silicon without diluent. When commercial silicon was used as a diluent, the large particle size and its high melting point caused to consume a lot of heat generated during ignition. Accordingly, the decrease of combustion temperature caused to complete the reduction reaction of silica duration 20 s. Therefore, there was not enough time for the silicon nuclei growth, leading to prepare branches with average diameter of 95 nm, smaller than 122 nm for branches prepared in the absence of diluent. In Fig. 3b, the large particles of commercial silicon and the small germinated nuclei of silicon are clear. When NaCl was used in reactant mixture, the rate of combustion reaction was controlled owing to its appropriate thermal conductivity and the explosion was homogenously distributed throughout the sample which is confirmed by Khanra *et al.* [19].

4. Conclusion: Nanocrystalline silicon with homogeneous coral-like morphology was successfully synthesised via mechanically activated SHS (MASHS) through diluent from as-synthesised SiO₂ cryogel. In MASHS method, the ignition reaction at optimised temperature of 1000°C led to nucleation and uniform growth of the branches in coral-like structure. The major grownup branches at this temperature had the diameter size distribution in the range of 100–150 nm with the average size of 122 nm. Moreover, 10 wt% NaCl as an efficient diluent because of its desirable thermal conductivity consumed the heat generated during exothermic reaction, inhibited the crystallite growth and enabled the formation of silicon with 10 Å° crystallinity. Furthermore, mechanism of crystalline growth and the branches growth under high combustion temperature was investigated. Silicon nanocrystals will steeply increase the yield of electronic device such as optoelectronic devices through its wide bandgap and high strain in its structure.

5. Acknowledgment: The authors acknowledge Materials and Energy Research Center (MERC) in Tehran, Iran for funding of this research.

6 References

- [1] Tian B., Zheng X., Kempa T.J., *ET AL.*: 'Coaxial silicon nanowires as solar cells and nanoelectronic power sources', *Nature*, 2007, **449**, pp. 885–889
- [2] Chan C.K., Peng H., Liu G., *ET AL.*: 'High-performance lithium battery anodes using silicon nanowires', *Nat. Nano*, 2008, **3**, pp. 31–35
- [3] Nersisyan H.H., Won H.I., Won C.W., *ET AL.*: 'Combustion synthesis of nanostructured tungsten and its morphological study', *Powder Technol.*, 2009, **189**, pp. 422–425
- [4] Guo X., Mao D., Wang S., *ET AL.*: 'Combustion synthesis of CuO–ZnO–ZrO₂ catalysts for the hydrogenation of carbon dioxide to methanol', *Catal. Commun.*, 2009, **10**, pp. 1661–1664
- [5] Yermekova Z., Mansurov Z., Mukasyan A.: 'Combustion synthesis of silicon nanopowders', *Int. J. Self-Propag. High-Temp. Synth.*, 2010, **19**, pp. 94–101
- [6] Merzhanov A.: 'History and recent developments in SHS', *Ceram. Int.*, 1995, **21**, pp. 371–379
- [7] Sytshev A.E., Merzhanov A.G.: 'Self-propagating high-temperature synthesis of nanomaterials', *Russ. Chem. Rev.*, 2004, **73**, pp. 147–159
- [8] Wen W., Wu J.-M.: 'Nanomaterials via solution combustion synthesis: a step nearer to controllability', *RSC Adv.*, 2014, **4**, pp. 58090–58100
- [9] Aruna S.T., Mukasyan A.S.: 'Combustion synthesis and nanomaterials', *Curr. Opin. Solid State Mater. Sci.*, 2008, **12**, pp. 44–50
- [10] Podbolotov K.: 'SHS in the Al–SiO₂–C system: the effect of additives', *Int. J. Self-Propag. High-Temp. Synth.*, 2010, **19**, pp. 244–252
- [11] Zaytsev A., Borovinskaya I., Vershinnikov V., *ET AL.*: 'Near-nano and coarse-grain WC powders obtained by the self-propagating high-temperature synthesis and cemented carbides on their basis. part I: structure, composition and properties of WC powders', *Int. J. Refract. Met. Hard Mater.*, 2015, **50**, pp. 146–151
- [12] Moore J.J., Feng H.: 'Combustion synthesis of advanced materials: part I. Reaction parameters', *Prog. Mater. Sci.*, 1995, **39**, pp. 243–273
- [13] Xu J., Zhang B., Jiang G., *ET AL.*: 'Synthesis of SiCw/MoSi₂ powder by the 'chemical oven' self-propagating combustion method', *Ceram. Int.*, 2006, **32**, pp. 633–636
- [14] Roghani H., Tayebifard S.A., Kazemzadeh A., *ET AL.*: 'Phase and morphology studies of B4C–SiC nanocomposite powder synthesized by MASHS method in B₂O₃, Mg, C and Si system', *Adv. Powder Technol.*, 2015, **26**, pp. 1116–1122
- [15] Subrahmanyam J., Vijayakumar M.: 'Self-propagating high-temperature synthesis', *J. Mater. Sci.*, 1992, **27**, pp. 6249–6273
- [16] Nadiradze A., Baratashvili I., Pulariani I., *ET AL.*: 'Thermodynamic probability of realization of the process of silicon dioxide reduction by magnesium at high temperatures', *Bull. Georg. Natl. Acad. Sci.*, 2009, **3**, pp. 95–99
- [17] Abbaschian R., Reed-Hill R.: 'Physical metallurgy principles', *Cengage Learn.*, 2008, pp. 769
- [18] Pons A., Casas L., Estop E., *ET AL.*: 'A new route to aerogels: monolithic silica cryogels', *J. Non-Cryst. Solids*, 2012, **358**, pp. 461–469
- [19] Khanra A., Pathak L.C., Mishra S.K., *ET AL.*: 'Effect of NaCl on the synthesis of TiB₂ powder by a self-propagating high-temperature synthesis technique', *Mater. Lett.*, 2004, **58**, pp. 733–738